Paper 107

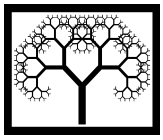

Proceedings of the Eighth International Conference on Engineering Computational Technology, B.H.V. Topping, (Editor), Civil-Comp Press, Stirlingshire, Scotland

Influence of Microscopic Factors on Lateral Earth Pressure using the Discrete Element Approach

M.-C. Weng and C.-C. Cheng
Department of Civil and Environmental Engineering
National University of Kaohsiung, Taiwan

Abstract

This study adopted the discrete element method (*DEM*) to explore the key influencing factors on the variations of lateral earth pressure, including packing type, interior friction angle, particle stiffness and particle size. The reference parameters for the *DEM* model were retrieved from direct shear tests of a rod assembly. Based on the reference parameters, the evolution of lateral earth pressure is further simulated, and a parametric study was conducted. The results showed that: (1) the analysis model could effectively capture the variation of lateral earth pressure under both active and passive conditions; (2) the greater interior friction angle $\phi_{interior}$ decreased the active coefficient K_a and increased the passive coefficient K_p; (3) increasing particle stiffness decreased the active coefficient K_a and increased the passive coefficient K_p; (4) larger particle sizes led to a larger active coefficient K_a and a smaller passive coefficient K_p; and (5) when the particle assembly was arranged in order, its lateral pressure was much larger than that of the randomly packed assembly.

Keywords: discrete element method, PFC2D,lateral earth pressure.

1 Introduction

In designing geotechnical structures such as retaining walls and structure foundations, the earth pressure is an important design parameter. Figure 1 shows a typical example of the earth pressure of a wall σ_h' versus the wall displacement ratio of the wall displacement ΔH to the wall height H [1]. It can be seen that the magnitude of earth pressure depends on the degree of movement of the wall. When the wall is at rest, the earth pressure at this moment is called the at-rest earth pressure. If the wall moves outward, i.e., it has a positive displacement ratio, the earth pressure on the wall decreases, and it will finally reach an active failure state. If the wall moves inward, i.e., it has a negative displacement ratio, the earth pressure

on the wall increases, and it will finally reach a passive failure state. Thus, the threshold of the wall displacement ratio in reaching either active or passive failure states depends on the soil type. Conventionally, the soil is idealized as a continuum to estimate the earth pressure. As an extreme case, the soil is further assumed to be rigid and only accounts for the equilibrium of forces, or works on a prescribed failure surface to compute the limit values of earth pressure in the active and passive states, i.e. active and passive earth pressure. For example, the well-known Coulomb's theory [2] was developed by adopting the limit equilibrium method to search for the most likely plane failure surface that produces an extreme earth pressure value. However, many researchers have found experimentally that the theory could not work well in some soils due to its assumption of ideal conditions [3-6]. In contrast, the finite element method (*FEM*) regards the soil as a deformable elastic-plastic continuum, and can be employed to determine the variation of earth pressure in relation to the wall movement as shown in Figure 1 [1, 7]. It should be pointed out that soils may not be described as a continuum. Like sands or gravels, they exhibit granular characteristics and have the property of particle separation. The failure pattern of granular materials is often sliding between particles, movements that cannot be interpreted by continuum mechanics. Therefore, it is of key interest to investigate the influence of inter-particle interactions on the development of earth pressure from the viewpoint of particle mechanics.

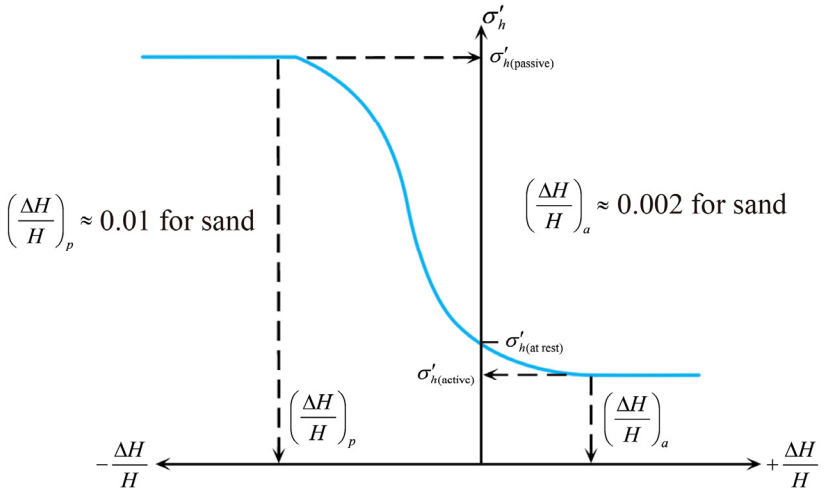

Figure 1 Variation of lateral earth pressure [1]

The discrete element method (*DEM*), proposed by Cundall [8-9], provides a feasible means to gain more insight into the relationships between the microscopic properties and the macroscopic behavior of granular materials. The *DEM* has been implemented in the software *PFC2D* and has been widely used to investigate the micro-deformation mechanisms and failure patterns of geo-materials [10]. This study used the DEM implemented in *PFC2D* to investigate the evolution of earth pressure under the plane strain condition, considering the soil as an assembly of particles. Preliminarily, the inter-particle bond and the pore water effect were ignored. Direct shear tests of aluminum-rod assemblies with different packing types

were conducted to deduce the reference microscopic properties for the *DEM* model. Then, based on the reference properties, a parametric study was performed to explore the influence of microscopic factors, including particle size, particle arrangement, and inter-particle stiffness and friction coefficients, on earth pressure. Additionally, the applicability of the *DEM* model for lateral earth pressure was validated using sandbox testing of aluminum-rod assemblies.

2 Contact model and required parameters

In *PFC2D*, a basic element represents a rigid circular disk with a finite mass. When one particle contacts with another or a boundary, the particle is allowed to slightly overlap at the contact point and the interaction between particles is described as a soft contact [10], which occurs over an infinitely small area. Therefore, a contact force is formed, and it is divisible into normal and shear components with respect to the contact plane. Herein, the linear contact model is adopted, and the normal force can be expressed as

$$F_i^n = k^n U^n \tag{1}$$

where U^n is the normal overlap and k^n is the contact normal stiffness.
Similarly, the increment of shear force is given by

$$\Delta F_i^s = -k^s \Delta U_i^s \tag{2}$$

where ΔU_i^s is the increment of tangential overlap and k^s is the contact shear stiffness.
Furthermore, the slip between two particles is allowed to occur when the maximum shear force equals the friction, that is $F^s = \mu F^n = tan\ (\phi_{interior})\ F^n$, where μ is the friction coefficient and $\phi_{interior}$ is the inter-rod friction angle.

According to the abovementioned contact model, three material parameters, the normal stiffness k^n, the shear stiffness k^s, and the surface friction coefficient between particles μ, are required. These parameters will be determined by simulating the deformation behavior of rod assemblies under a series of direct shear tests.

2.1 Direct shear test of aluminum-rod assemblies

Considering the uniform geometry and homogeneity of particles, equal-sized circular aluminum rods were selected as the material for the direct shear test. Each rod was 6 mm with precision of 0.1 mm in diameter and 60 mm in length; the material density was 2702 kg/m^3; the Young's modulus was 70 GPa; the Poisson's ratio was 0.33. Furthermore, each test specimen had a square cross-section containing six layers of rods, with each layer including 10 rods. Dense packing of

particles with a porosity of 9.32% was conducted as shown in Figure 2. In order to investigate the influence of normal stress, four levels of normal stress were applied: 27.24, 54.48, 108.96 and 217.93 kg/cm^2. Following this, the specimens under different normal stress levels were sheared at a rate of 1 mm/min, based on the ASTM D3080-90 code. For measuring the deformation of each specimen, dial gauges were set up to obtain the horizontal and vertical deformation with a precision of 0.01 mm. The shear load was measured by a proving ring attached to the loading frame with an accuracy of 0.003 kg/cm^2.

Figure 2b illustrates a DEM model for simulation of direct shear tests. The specimen of a rod assembly was enclosed by the rigid boundaries. The lateral and lower boundaries were set rigid. The upper boundary was also rigid but allowed to tilt, and it was composed of a series of ball elements with high bond strength and stiffness. During shearing, the lower section of the box was moved forward at a constant velocity the same as the actual test, while the upper section of the box remained stationary. The required parameters were determined by comparing the results of a series of direct shear tests with the simulated results. Through several iterations, a set of microscopic model parameters was determined to ensure that the simulated macroscopic deformational behavior and strength were consistent with the experimental conditions.

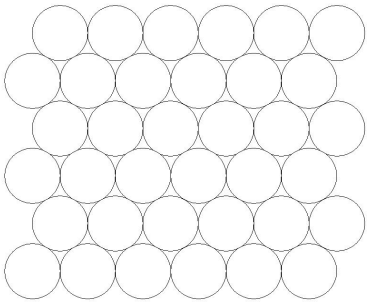

(a) dense packing of particles

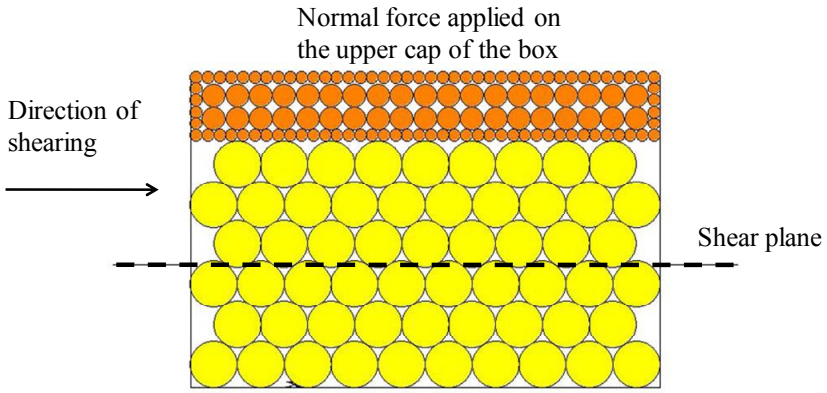

(b) Analysis model of direct shear test

Figure 2 Schematic diagram of dense packing of particles and the analysis model of direct shear test.

2.2 Verification of contact model

Figure 3 shows the stress-displacement curves of the dense packing condition obtained by experiment and numerical simulation. It can be seen the simulated and experimental curves under different normal pressure levels shown in Figure 3a were fairly consistent and the values of peak strength were also similar. Both the simulated and actual behaviors of the aluminum-rod assembly revealed that shear displacements increased linearly at the early shearing stage, and the stiffness increased with increasing application of normal pressure. When the shear stress approached the failure state, strain-softening behavior was observed and stress dropped gradually after the peak. The simulations of volumetric deformation were also similar to the experiment results as shown in Figure 3b, and all vertical displacement curves tended to be dilative during the whole shearing process. Accordingly, the set of parameters shown in Table 1 was determined as the reference parameters to be used for the subsequent parametric analysis.

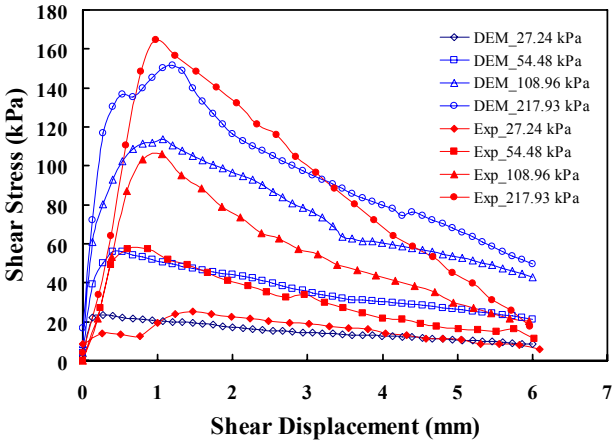

(a) Shear stress versus shear displacement

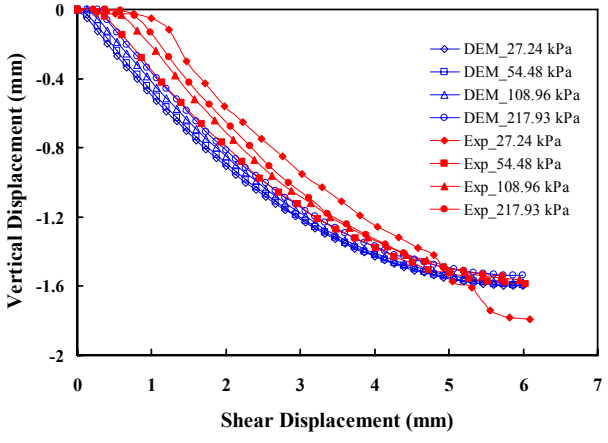

(b) Vertical displacement versus shear displacement

Figure 3 Comparison of simulated and actual deformations of the rod assembly with dense packing subjected to shearing under various hydrostatic stresses.

Property	Value (units)
Density	2702 kg/m^3
Normal stiffness k^n	10.35 MN/m
Shear stiffness k^s	1.95 MN/m
Inter-rod friction angle $\phi_{interior}$	20.9°

Table 1 Microscopic properties of particles for DEM analysis

The strength of the rod assembly was also determined using the Mohr-Coulomb expression as follows

$$\tau_f = \sigma \tan\phi + c \tag{3}$$

where τ_f and σ are the shear strength and normal stress respectively, and the parameters ϕ and c are the macroscopic friction angle and the cohesive intercept of the failure envelope, respectively.
For dense packing, the failure envelope is nearly linear with no cohesion and can be expressed as:

$$\tau_f = \sigma \tan 45.9° \tag{4}$$

With the above strength parameters, the coefficients of earth pressure for active and passive states based on the conventional plastic theory were evaluated, as presented in the following section.

3 DEM model for lateral earth pressure study

Based on the contact model and parameters described above, this study further explored the influences of different packing and microscopic properties of cohesion-less particles on the variations of lateral earth pressure. For dense packing, for example, a numerical model containing 20 layers of rods, each has 100 rods was constructed, as shown in Figure 4. The left side and the bottom of the model were considered as rigid boundaries, and the top of the model was set as an unconstrained boundary. For the right side of the model, a moveable boundary was adopted to simulate the movement of the wall. As the wall moved to the right, the earth pressure would develop an active state; as the right wall moved to the left, the earth pressure would develop a passive state. In this simulation, the wall was moved at a constant velocity of 0.1 mm/s. For considering the influence of particle packing, two

types of packing, dense packing and random packing, of which the porosities were about 20.7 %, were investigated. Based on these packing types, numerical analyses with different inter-particle friction angles, stiffness values, and rod sizes were conducted to systematically study the corresponding variations in earth pressure. The interior friction angle was chosen from the range ($\psi_{interior}$ -5°) to ($\psi_{interior}$ +20°), in which the corresponding friction coefficient ranged from 0.284 to 0.865. The normal stiffness ranged from 0.1 k^n to 100 k^n, of which the magnitude was between 1.035 MN/m to 1035 MN/m, considering the variety of deformation modulus of geo-material. To explore the size effect, four rod diameters were chosen as 1.5 mm, 3 mm, 6 mm and 12 mm.

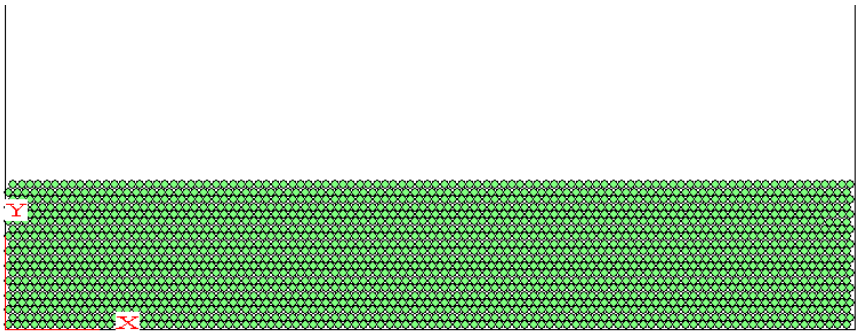

Figure 4 Schematic illustration of lateral earth pressure test.

4 Simulations and results

Figure 5 compares the variation of the earth pressure coefficient K_h from the *DEM* analysis with Coulomb's theory using $\phi = 45.9°$. It can be seen that under the active condition (Figure 5a), the values of K_h at large displacement were close to those from the Coulomb's theory. However, under the passive condition, a significant difference was found between the *DEM* analysis and Coulomb's theory. The peak value of the *DEM* analysis was much greater than that based on Coulomb's theory, with value is 2.48. For random packing as shown in Figure 5(b), it can be seen that for the passive state, the value of K_h at large displacement agreed well with that from Coulomb's theory, while for the active state, the value of K_h at large displacement was a little higher than that from Coulomb's theory. The overall agreement was fairly good. From the above comparisons, Coulomb's theory seems to be only suitable for the random packing of particles. As the particles became arranged in order, Coulomb's theory would underestimate the passive earth pressure.

Based on the simulation of lateral earth pressure, this study was able to further validate the adopted *DEM* model and use the associated model parameters as reference values in the parametric study described in the following section.

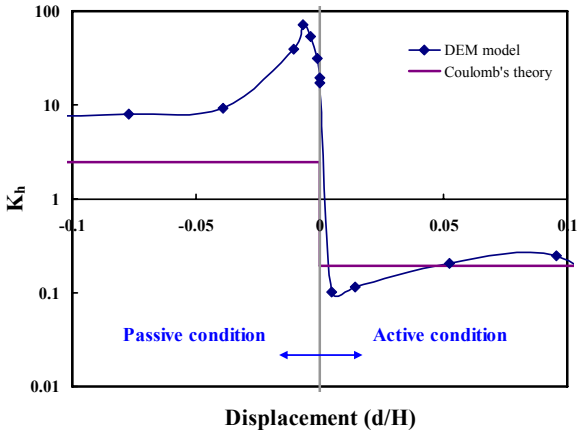

(a) Dense packing

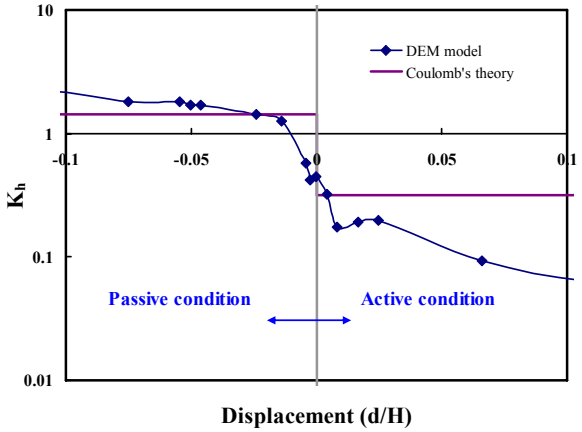

(b) Random packing

Figure 5 Variations of coefficient of lateral earth pressure under different packing conditions.

5 Influencing factors on the coefficients of earth pressure

The influence of microscopic factors, including particle arrangement, interior friction angle, stiffness, and particle size on the active and passive earth pressure coefficients are investigated in this section.

5.1 Influence of interior friction angle

Figure 6 depicts the variations of the earth pressure coefficients with different interior friction angles of particles, ranging from 15.8° to 40.8°. The theoretical results of Coulomb's theory are also plotted for comparison. For the active condition as shown in Figure 6a, it could be seen that increasing interior friction angle $\phi_{interior}$ decreased the active coefficient K_a in all packing types. These tendencies agree with that of Coulomb's theory, especially for the variation of random packing, which is much more similar to that of Coulomb's theory.

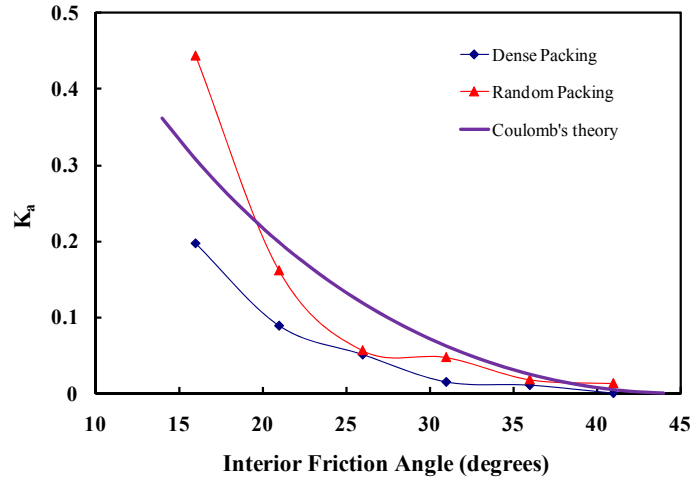

(a) Active condition

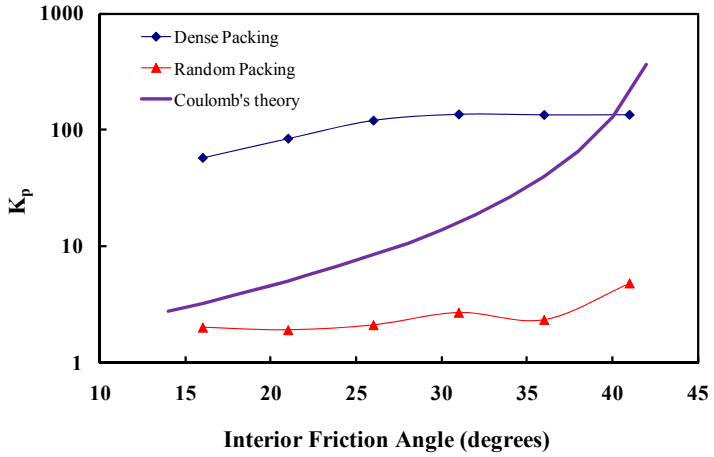

(b) Passive condition

Figure 6 Variation of the coefficient of lateral earth pressure with different friction angles.

On the other hand, an increase in $\phi_{interior}$ led to an increase in the passive coefficient K_p as shown in Figure 6b. Although the tendencies of variation were similar, the magnitudes of dense packing were much greater than that of random packing. For this packing type, owing to the particles arrangement in order, the contact forces between particles could completely develop and the exhibited resistant force became much larger. Furthermore, it was found that Coulomb's passive pressure exhibited a very wide range of variation. The Coulomb pressure was similar to that of random packing at a low friction angle (about 15°), and it increased rapidly and approached the values of dense packing at a high angle (after 38°). These results indicate that the tendencies of the two analysis methods are similar, but the coefficient values of earth pressure are apparently different.

5.2 Influence of stiffness

Figure 7 illustrates the variations of the earth pressure coefficients with different particle stiffness. For the active condition as shown in Figure7a, increasing particle stiffness decreased the active coefficient K_a in all packing types. Furthermore, an increase in the stiffness led to an increase in the passive coefficient K_p as shown in Figure7b. Conventionally, the earth pressure evaluation of limit equilibrium theory depends only on the friction angle, the cohesion, and the density of geo-material and it does not consider the deformation of geo-material. However, in this study, it was found that the magnitude of earth pressure is significantly affected by the stiffness, as shown in Figure 7. As compared to the influence of the friction angle, the particle stiffness seems more significant.

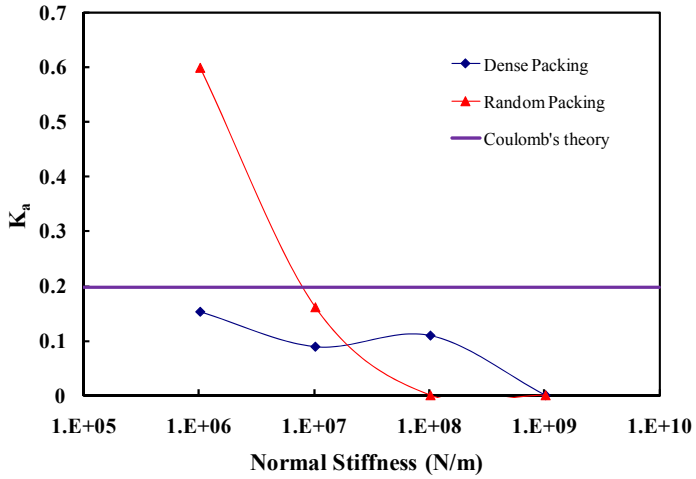

(a) Active condition

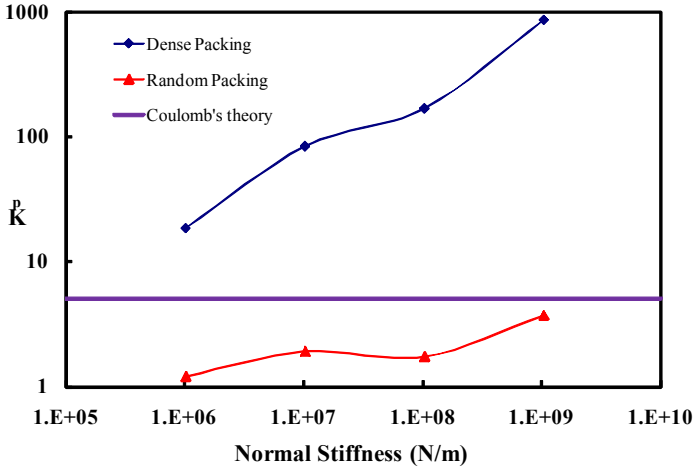

(b) Passive condition

Figure 7 Variation of the coefficient of lateral earth pressure with different particle stiffness.

5.3 Influence of particle size

Figure 8 illustrates the simulated earth pressure coefficient versus different particle sizes. Figure 8a shows how the active coefficient K_a of dense packing increased as the particle size increased. Especially for the random packing, the coefficient K_a is significantly influenced by the particle size. For the passive condition as shown in Figure 8b, the larger size induced the lower passive coefficient K_p.

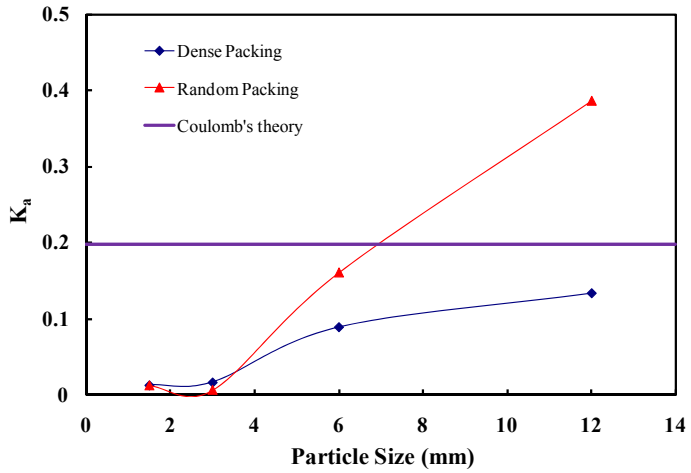

(a) Active condition

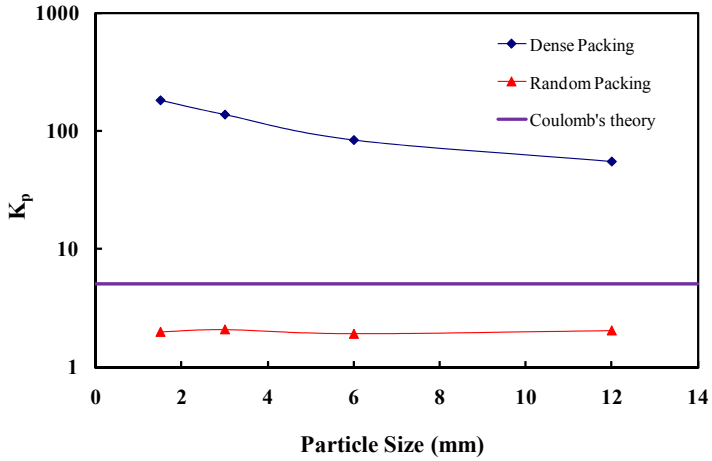

(b) Passive condition

Figure 8 Variation of coefficient of lateral earth pressure with different particle sizes.

6 Conclusions

This study explored the influencing factors, including the packing type, the interior friction angle, the particle stiffness and the particle size, on the variations of lateral

earth pressure. The software *PFC2D* based on the discrete element method (*DEM*) was adopted. The *DEM* model was tested for modeling direct shear tests and showed good capability in simulating and predicting the macroscopic mechanical behavior of a rod assembly under different stress states. On such a basis, the lateral earth pressure evolution was further simulated by the *DEM* model and the simulation results showed the following:

(1) The greater interior friction angle $\phi_{interior}$ led to the lower active coefficient K_a and increased the passive coefficient K_p. These tendencies agreed with that of the conventional limit equilibrium theory, but the values of the two analysis methods exhibited significant differences.

(2) Increasing inter-particle stiffness decreased the active coefficient K_a and increased the passive coefficient K_p. The larger particle size led to the higher active coefficient K_a and the lower passive coefficient K_p

(3) When the assembly was arranged in order, such as dense packing, it exhibited much larger lateral pressure than for the random packing.

The packing type, particle stiffness and particle size are not considered in the conventional limit equilibrium theory. The *DEM* analysis in this study has shown that these factors indeed affect the evolution of lateral earth pressure.

Acknowledgements

The research is partly supported by the National Science Council of Taiwan, Grant no. NSC-100-2221-E-390 -022.

References

[1] B.M. Das, “Principles of Foundation Design”, Brooks/Cole Publishing Company, 2010.

[2] C.A. Coulomb, “Essai sur une Application des Regles de Maximis a quelques Problems de Statique, relatifs a l’Architecture”, Mem. Roy. Des Science, Paris, 3(38), 1776.

[3] R.D. Mackey, D.P. Kirk, “At rest, active and passive earth pressure”, Proc. South East Asian Conf. on Soil Mechanics and Foundations Engineering, Bangkok, 187–199, 1967.

[4] J. Naraun, S. Saran, P. Nandakumaran, “Model study of passive pressure in sand”, J Soil Mech Found Div ASCE, 95(4), 969–983, 1969.

[5] Y.S. Fang, Y.C. Ho, T.J. Chen, “Passive earth pressure with critical state concept”, J Geotech Geoenviron Eng, 128(8), 651–659, 2002.

[6] C.C. Hung, F.Y. Menq, Y.C. Chou, “The effect of the bending rigidity of a wall on lateral pressure distribution”, Can Geotech J, 36, 1039–1055, 1999.

[7] H. Matsuzawa, H. Hazarika, “Analyses of active earth pressure against rigid retaining wall subjected to different modes of movement”, Soils and Foundations, 36(3), 51-65, 1996.

[8] P.A. Cundall, O.D.L. Strack, “A discrete numerical model for granular assemblies”, Geotechnique, 29(1), 47–65, 1979.
[9] P.A. Cundall, “A computer model for simulating progressive, large scale movement in blocky rock systems”, Proc., Symp. Int. Soc. Rock Mech., Inst. Civ. Engrg., Nancy, France., 2(8), 129–136, 1971.
[10] PFC2D (Particle Flow Code in 2 Dimension). Version 4.0. Minneapolis: Itasca Cons Group, 2004.